Cyclic tests of steel frames with composite lightweight infill walls

Hetao Hou[1a], Chung-Che Chou[*2], Jian Zhou[1], Minglei Wu[3], Bing Qu[1,4], Haideng Ye[1], Haining Liu[1] and Jingjing Li[1]

[1]*School of Civil Engineering, Shandong University, Jinan, Shandong, 250061, P.R. China*
[2]*Department of Civil Engineering, National Taiwan University, 10617, Taipei, Taiwan*
[3]*Shandong Engineering Consulting Institute, Jinan, Shandong, 250013, P.R. China*
[4]*Department of Civil and Environmental Engineering, California Polytechnic State University, San Luis Obispo, CA 93407, USA*

Abstract. Composite Lightweight (CL) insulated walls have gained wide adoption recently because the exterior claddings of steel building frames have their cost effectiveness, good thermal and structural efficiency. To investigate the seismic behavior, lateral stiffness, ductility and energy dissipation of steel frames with the CL infill walls, five one-story one-bay steel frames were fabricated and tested under cyclic loads. Test results showed that the bolted connections allow relative movement between CL infill walls and steel frames, enabling the system to exhibit satisfactory performance under lateral loads. Additionally, it is found that the addition of diagonal steel straps to the CL infill wall significantly increases the initial lateral stiffness, load-carrying capacity, ductility and energy dissipation capacity of the system. Furthermore, the test results indicate that the lateral stiffness values of the frames with the CL infill wall are similar to those of the bare steel frames in large lateral displacement.

Keywords: composite lightweight infill wall; steel frame; bolted connection; cyclic test; energy

1. Introduction

Composite Lightweight (CL) insulated walls have gained wide adoption recently because the exterior claddings of steel frame buildings have their cost effectiveness, good thermal and structural efficiency. A typical CL infill wall consists of two concrete panels that are separated by an insulation core (Fig. 1(a)); the concrete panels are connected by truss-type shear connectors that penetrate the insulation core (Benayoune *et al*. 2008, Hou *et al*. 2009). Although the CL walls are gradually used as infills in steel building frames, research on their seismic performance is very limited and no design guidelines are available for implementing this system.

Through experimental research on steel frames with CL infill walls, some researchers discovered that the infill wall can considerably enhance the lateral stiffness, ultimate strength and

---

∗Corresponding author, Professor, E-mail: cechou@ntu.edu.tw
[a]Associate Professor, E-mail: houhetao@sdu.edu.cn

hysteretic energy dissipation capacity of the system (Wallace and Wada 2000, Tong *et al.* 2005, Lee and Ko 2007, Le 2014). Aliaari and Memari (2005) developed a seismic masonry wall that was isolated from a building frame. The analytical results showed that such a wall initially had a high lateral stiffness followed by isolation from the confining frame with the increase of lateral loads. Moreover, the masonry walls infilled in a reinforced concrete frame structure decreased the maximum inter-story drift while increasing the hysteretic energy dissipation capacity of the frames. Hence, neglecting the contribution of the masonry infills would be inappropriate when evaluating the seismic performance of surrounding frame structures (El-Sokkary and Galal 2009). Sun *et al.* (2011) performed quasi-static cyclic tests to investigate the behavior of a one-bay, two-story partially-restrained steel frame with reinforced concrete infill walls. Test results showed that the wall-frame system had good lateral stiffness and strength under cyclic loads. Fang *et al.* (2013) conducted shaking table tests to study the seismic behavior of a two-story steel frame with Autoclaved Lightweight Concrete (ALC) wall panels. The wall panels experienced minor damage, and the joints between the ALC panel and the steel frame were able to resist large seismic loads. The ALC panels increased the system lateral stiffness and damping ratio by 25% and 7%, respectively.

Past works, as reviewed above, mainly focused on steel frames infilled with masonry walls, reinforced concrete walls or ALC walls. Very limited works are available on the seismic behavior of the steel frames with CL infill walls. Particularly, knowledge gaps exist regarding the interaction between the steel frame and the CL infill walls and the contribution of adding diagonal steel straps to the CL infill wall for improving the seismic performance. This paper addresses the issues of the CL infill wall on the test performance of the steel frame under cyclic loads. Five one-story one-bay steel frames with different infill walls and wall-to-frame connections were tested to examine their failure modes, ductility capacity, hysteretic energy dissipation capacity, stiffness and strength degradation under lateral cyclic loads.

2. Test program

The test program consisted of cyclic testing of five specimens. This section presents specimen details and the loading protocol used in the study. Four one-story, one-bay specimens with different types of CL infill walls but identical boundary frames (Specimens SF1 to SF4 in Table 1) were first tested. Then, a bare frame specimen that was the same as the boundary frame of those specimens with CL infill walls (Specimen SF5 in Table 1) was tested to provide reference data of the seismic performance of the bare frame. These tests could be used to examine the cyclic behavior of the CL-infill wall installed in the frame and to validate the seismic performance of the steel wall-frame system.

2.1 Specimen description

Table 1 lists test parameters for the specimens, which include material properties of the CL infill walls, locations of wall-to-frame connections, and if diagonal steel straps were added. Specimen SF1 positioned steel connectors at the top and bottom of the columns to assemble a normal-weight infill wall and a steel frame (Fig. 1(b)). Frame members were designed for gravity and seismic loading. The column and beam members were HW150×150×7×10 mm and HN150×75×5×7 mm, respectively. Table 2 summarizes tensile test results of steel coupons for the

Table 1 Specimen test parameters

Specimen ID	Connector Location	Type of Infills	Type of Concrete
SF1	Column Bottom & Top	Wall only	Normal
SF2	Column Bottom & Beam Bottom	Wall only	Normal
SF3	Column Bottom & Beam Bottom	Wall only	Ceramic Concrete
SF4	Column Bottom & Beam Bottom	Wall and Steel Straps	Normal
SF5	N.A.	N.A.	N.A.

Table 2 Properties of steel

Thickness (mm)	Yield Strength (MPa)	Ultimate Strength (MPa)
5	272	370
7	290	396
8	294	399
10	302	414
12	299	409
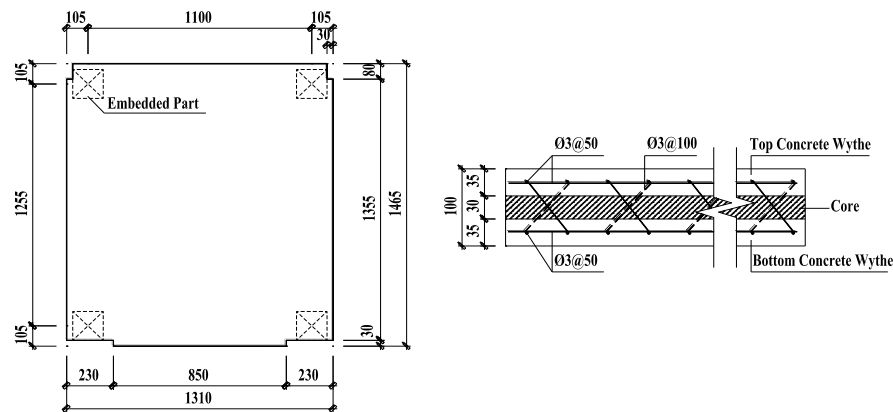
(a) Cross Section and Elevation of the CL wall
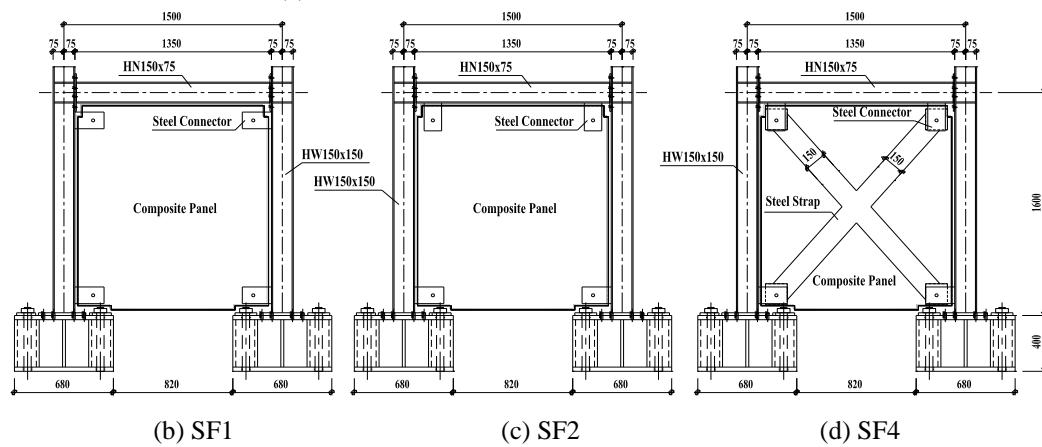
(b) SF1   (c) SF2   (d) SF4

Fig. 1 Specimen details

flanges and webs of the frame members. The beams and columns were assembled using semi-rigid connections, in which eight 16 mm-diameter bolts were used to connect a 12 mm-thick end plate of the beam and the column flange (Fig. 2). Each column was mounted to the laboratory strong floor by four post-tensioning rods.
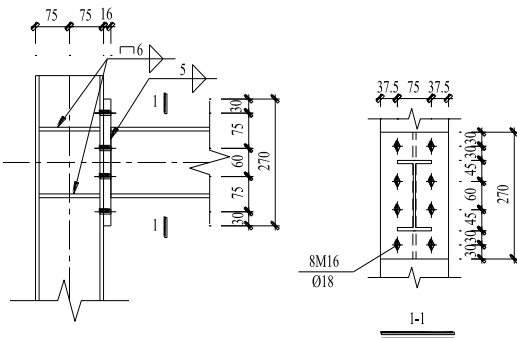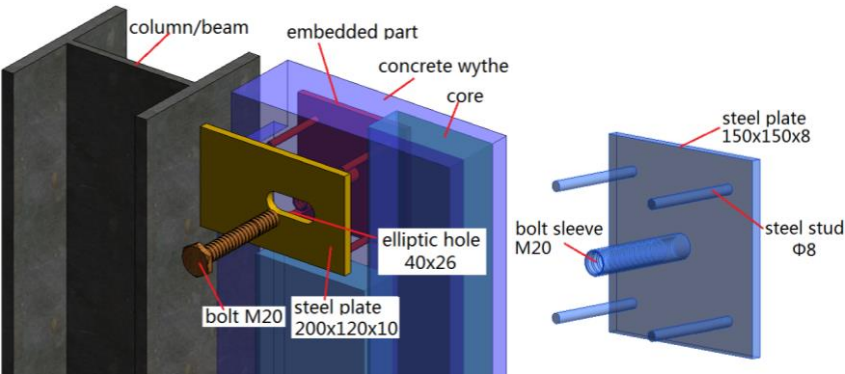

Fig. 2 Semi-rigid beam-to-column connection

Fig. 3 CL infill wall-to-frame connection

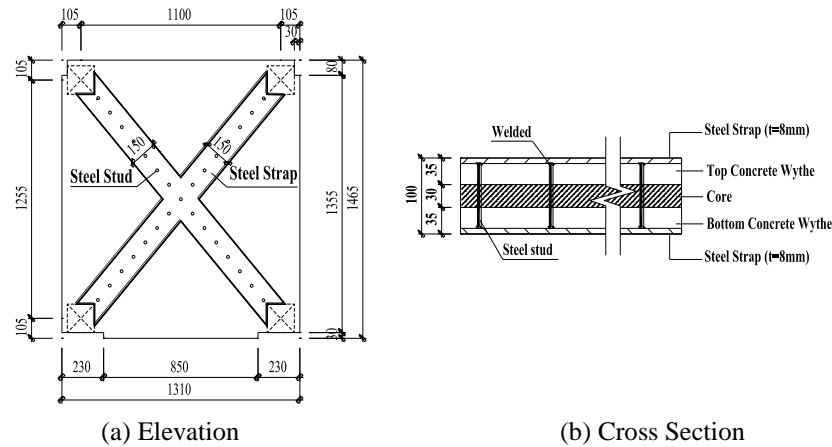(a) Elevation   (b) Cross Section

Fig. 4 Specimen SF4 (CL Infill Wall with Steel Straps)

Fig. 3 presents connection details between the steel frame and the CL-infill wall; a Q235B connector plate (200×120×10 mm) that was welded to the column or beam member was used to connect the CL infill wall by a M20 mm-diameter high-strength bolt. An elliptic bolt hole with the length and width of 40 mm and 26 mm, respectively, was adopted in the infill-wall-to-boundary-frame connection (see Fig. 3) to allow relative movement between the infill-wall and the frame under cyclic loads. An 8 mm-thick steel plate that was placed on the opposite side of the connector plate was used to provide confinement to corner concrete. Depending on different construction practices, the connection assemblage was positioned at either the column top (Fig. 1(b)) or the beam bottom flange (Fig. 1(c)). All specimens except for Specimen SF1 (Fig. 1(b)) were designed to connect the CL infill wall to the beam bottom flange and the bottom of the column. Moreover, Specimens SF1, SF2, and SF4 used normal-weight concrete infill walls and Specimen SF3 used a ceramic concrete infill wall, in which normal-weight coarse aggregates were replaced by shale ceramic aggregates. The density of ceramic concrete was 1838 kg/m^3, less than 2413 kg/m^3 of normal-weight concrete. The objective of using ceramic concrete was to reduce the weight of the CL-infill for application. On the day of testing, the average compressive strength of normal-weight concrete and ceramic concrete was 32 and 52 MPa, respectively. The measured elastic modulus of normal-weight concrete and ceramic concrete were 3.93×10^4 N/mm^2 and 2.43×10^4 N/mm^2, respectively. The strength of ceramic concrete was higher than that of normal-weight concrete owing to a smaller water-cement ratio for the ceramic concrete. Additionally, Specimen SF4 added two 8 mm-thick steel straps on both sides of the CL infill wall (Fig. 1(d) and Fig. 4) to enhance the shear force transfer of the wall and delay premature failure of the wall. The steel straps were bonded to the CL infill wall by using 8 mm-diameter steel studs.

The lateral stiffness of the entire frame, D_i, is the summation of the lateral stiffness of the bare frame, D_f, and that of the infill wall, D_d (Cavaleri and Trapani 2014)

$$D_d = \frac{k_d \cos^2 \theta}{1 + \frac{k_d}{k_c} \sin^2 \theta} \tag{1}$$

$$k_d = E_d tw / d \tag{2}$$

$$k_c = E_f A_c / H \tag{3}$$

where k_d and k_c are the axial stiffness values of the equivalent diagonal strut and the steel column, respectively; E_d and E_f are the elastic modulus of the equivalent diagonal strut and steel, respectively; t is the thickness of the wall; w is the width of the equivalent diagonal strut; A_c is the cross sectional area of the steel column; H is the height of the steel frame; d is the diagonal length of the wall, and θ is the angle of the diagonal strut. The lateral stiffness of the wall can also be expressed (Carrillo and Alcocer 2013)

$$D_d = \frac{1}{\dfrac{h^3}{3c_1 EI} + \dfrac{h}{1.2c_2 GA}} \tag{4}$$

where c_1 and c_2 are factors accounting for cracking of concrete prior to yielding of reinforcement (here c_1=0.07, c_2=0.05); E is the elastic modulus of the wall material; h is the height of the wall; A and I are the cross-sectional area and moment of inertia of the wall, respectively, and G is the shear modulus of wall material. The lateral stiffness values of a wall, expressed by Eqs. (1) and (4), respectively, were assumed to be the same, leading to a value of 124 mm for the width of the equivalent diagonal strut, w. Therefore, the width and thickness of the steel straps in Specimen SF4 were 150 mm and 8 mm, respectively. Two steel straps were connected to each other along the diagonal direction by using 8 mm-diameter steel studs with a spacing of 100 mm (Fig. 4). The steel straps were Q235B steel with a normal yield strength of 294 MPa.
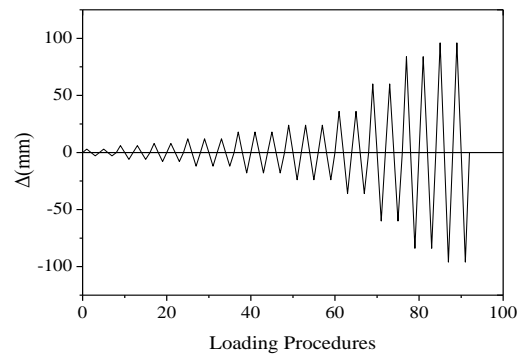
The shear strength and tensile strength of a M20 bolt that was used to connect the CL infill wall and the boundary frame were 42 kN and 124 kN, respectively. The elastic inter-story drift of the moment-resisting frame under lateral loads was limited to 0.4% according to the Chinese Code for Seismic Design of Buildings (GB50011-2010). The shear force that was applied to the wall at the elastic inter-story drift of 0.4% was 141 kN, calculated based on Eq. (4). Therefore, the shear force to each infill-wall-to-boundary-frame connection was 35 kN, which was less than the shear strength of a M20 bolt and unconfined concrete bearing strength. The elliptic hole was 26×40 mm that allowed a relative movement of 10 mm when the bare steel frame reached a yield displacement level, Δ_y, of 12 mm.

2.2 Loading protocol

The same test setup was used for all specimens. Fig. 5(a) shows Specimen SF2 in the test setup; Fig. 5(b) shows the loading protocol adopted in this study which was determined based on the ATC-63 guidelines (ATC 2009). The loading history that was composed of elastic and inelastic cycles was applied to specimens in displacement control. The elastic cycles had displacement levels of $0.25\Delta_y$, $0.5\Delta_y$ and $0.7\Delta_y$, where Δ_y was the lateral yield displacement corresponding to the lateral yield load P_y. In this study, Δ_y was about 12 mm based on the numerical analysis of the bare steel frame using the computer program ABAQUS (ABAQUS 2009). The specimens were loaded two cycles for displacement levels lower than Δ_y. The inelastic cycles had displacement levels of Δ_y, $1.5\Delta_y$, $2\Delta_y$, $3\Delta_y$, and $5\Delta_y$. The specimens were loaded three cycles for displacement levels from Δ_y to $2\Delta_y$, and two cycles for each of the other inelastic displacement levels. The test was paused

(a) Specimen SF2 before Test   (b) Loading Protocol

Fig. 5 Specimen SF2 and loading protocol

after every two cycles at the specified displacement so that the progress of damage in the CL-infill wall and the steel frame could be examined. The test was stopped when the specimen failed. For the bare steel frame test (Specimen SF5), the actuator was only driven to a displacement level that was less than the expected elastic limit Δ_y to prevent damage from the steel frame and to ensure its adequacy for reuse in the following tests.

2.3 Instrumentation plan

The beam end displacement was recorded by the actuator. In addition, seven linear variable displacement transducers (LVDTs) were used to measure the displacement of the wall, slippage of the column base, and out-of-plan motion of the specimens. Moreover, a total of 58 strain gauges were employed in each specimen to measure strains of the CL infill wall, steel connector, beams and columns, respectively.

3. Discussion of test results

The test results of the specimens with CL infill walls (Specimens SF1 to SF4) were presented and compared with those obtained from the bare steel frame (Specimen SF5). Discussion was focused on the cyclic behavior, lateral stiffness, hysteretic energy dissipation and force *versus* displacement responses of the specimens with the CL infill wall.

Damage pattern and crack propagation of the CL infill walls were similar in all specimens with infills except for Specimen SF4, so the observed performances of Specimens SF2 and SF4 are

(a) Crack at Left-Top Corner   (b) Splitting at Left-Bottom Corner

(c) Crushing at Left-Bottom Corner (Back Side)   (d) Buckling of Beam Top Flange

Fig. 6 Performance of Specimen SF2

presented in the following. These two specimens used the same steel connectors welded at the beam bottom flange and the column bottom for assembling the steel frame and the CL infill wall except that Specimen SF4 had two additional steel straps bonded to both sides of the wall (Table 1). When the beam end displacement of Specimen SF2 reached the first cycle of $0.25\Delta_y$, short and small cracks appeared near the left-top corner of the CL-infill wall (Fig. 6(a)). These cracks propagated with the increase of the beam end displacement. When the beam end displacement reached 8.4 mm (=$0.7\Delta_y$), sliding between the steel connector and the bolt was noticed. A rigid connection between the CL infill wall and the frame was maintained only in a low drift range (i.e., 0-$0.25\Delta_y$). The response associated with a larger drift range (i.e., 0.25-$0.7\Delta_y$) was used to evaluate the elastic stiffness of the systems with CL infill walls. During the loading cycle of $1.5\Delta_y$ (18 mm displacement at the beam end), the concrete crack width was 6 mm and concrete spalling was observed at the right-top corner. At the second cycle of $3\Delta_y$, specimen made a rattling sound that was caused by friction between the steel connector and the CL infill wall. A 40 cm-long crack appeared in the middle of the wall surface, and concrete spalling was observed at the left-bottom corner of the CL infill wall. When the beam end displacement reached the first cycle of $5\Delta_y$, concrete splitting and crushing were found near both sides of the left-bottom corner (Fig. 6(b) and (c)). The beam top flange experienced minor buckling at this deformation level (Fig. 6(d)), causing a drop of the peak strength. Although the steel frame worked with the CL infill wall to resist lateral

(a) Minor Concrete Crack ($0.7\Delta_y$) (b) Concrete Crush ($5\Delta_y$)

(c) Lateral Movement of the Wall ($5\Delta_y$) (d) Column Twisting ($5\Delta_y$)
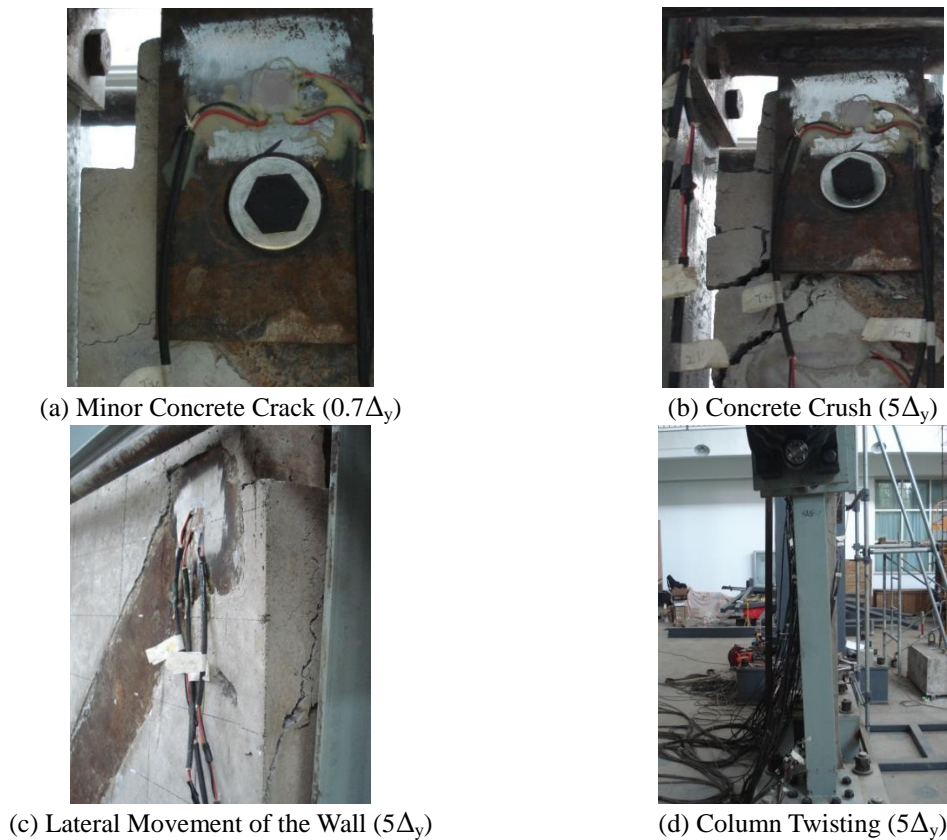
Fig. 7 Performance of Specimen SF4

loads, most damage was found in the CL infill wall, especially for concrete around the steel connectors. No separation was found between the CL infill wall and the steel frame after the test. The steel frame experienced minor buckling of the beam, but no failure was observed in the frame members or beam-to-column connections, indicating that the frames with CL infill walls could be a viable earthquake resisting system.

Specimen SF4 was designed with steel straps to provide improved integrity of the CL infill wall under cyclic loads. When the beam end reached the first cycle of $0.25\Delta_y$, small cracks occurred along both edges of the steel strap, indicating force transfer through the bond between concrete and steel straps. Cracks were found only near corners of the CL infill wall when the beam end displacement was from $0.5\Delta_y$ to $2\Delta_y$ (Fig. 7(a)). The left-top concrete corner spalled at the beam end displacement of $3\Delta_y$; the damage was more severe than that of Specimen SF2 at the same drift level. However, many minor cracks were observed in the wall except for corners, indicating that the steel straps could resist some shears to delay damage of the CL infill wall. When the beam end displacement reached the first cycle of $5\Delta_y$ (=60 mm), corners of the CL-infill wall crushed (Fig. 7(b)), leading to out-of-plan movement of the CL-infill wall (Fig. 7(c)). The behavior was not observed in other specimens during the tests. At the second cycle of $5\Delta_y$, buckling of the beam top flange occurred, leading to twisting of the steel column (Fig. 7(d)).

3.1 Force versus displacement relationship

Fig. 8 shows the hysteretic responses of specimens with CL infill walls. The CL-infilled frame was ductile because the wall-frame system could reach large inelastic deformation without significant strength degradation except for the last drift cycle. As the drift increased, pinching became significant because of damage in the wall corners and slippage between the wall and the frame. In all specimens, the peak resistance in the first loading cycle of each drift level was observed to be higher than that of the subsequent cycle due to the cumulated concrete damage. Specimens SF1 and SF2 showed similar hysteretic responses (Fig. 8(a) and (b)), indicating that the steel connectors that were welded either at the beam bottom flange or the column top to assemble the CL infill wall and the frame did not have significant impacts on the wall behavior. Based on hysteretic responses of Specimens SF2 and SF3 (Fig. 8(b) and (c)), the ceramic concrete wall exhibited narrower response but similar damage compared to the normal-weight concrete wall. Although the normal-weight concrete and the ceramic concrete were used in Specimens SF2 and SF3 (Table 1), respectively, the maximum strengths of both specimens were similar. The hysteretic response of Specimen SF4, which used steel straps to bond the CL infill wall, showed the largest strength and energy dissipation among all specimens (Fig. 8(d)), indicating that some shear can be resisted by the steel straps. The maximum strength of Specimen SF4 was increased by 8% in comparison to that of Specimen SF2.

Fig. 9 shows backbone curves of specimens with CL infill walls. Except for the last cycle, specimens loaded in either positive or negative directions did not exhibit noticeable strength degradation. Although the CL infill wall experienced spalling of corner concrete and slippage between the steel connectors and the wall, the specimen strength increased with drift. Except for Specimen SF4 with steel straps to enhance the shear resistance of the wall, Specimen SF1 that located steel connectors at the column top and bottom to connect the CL infill wall showed the maximum strength among Specimens SF1, SF2, and SF3, probably due to less deformation in the column top than in the beam bottom side.
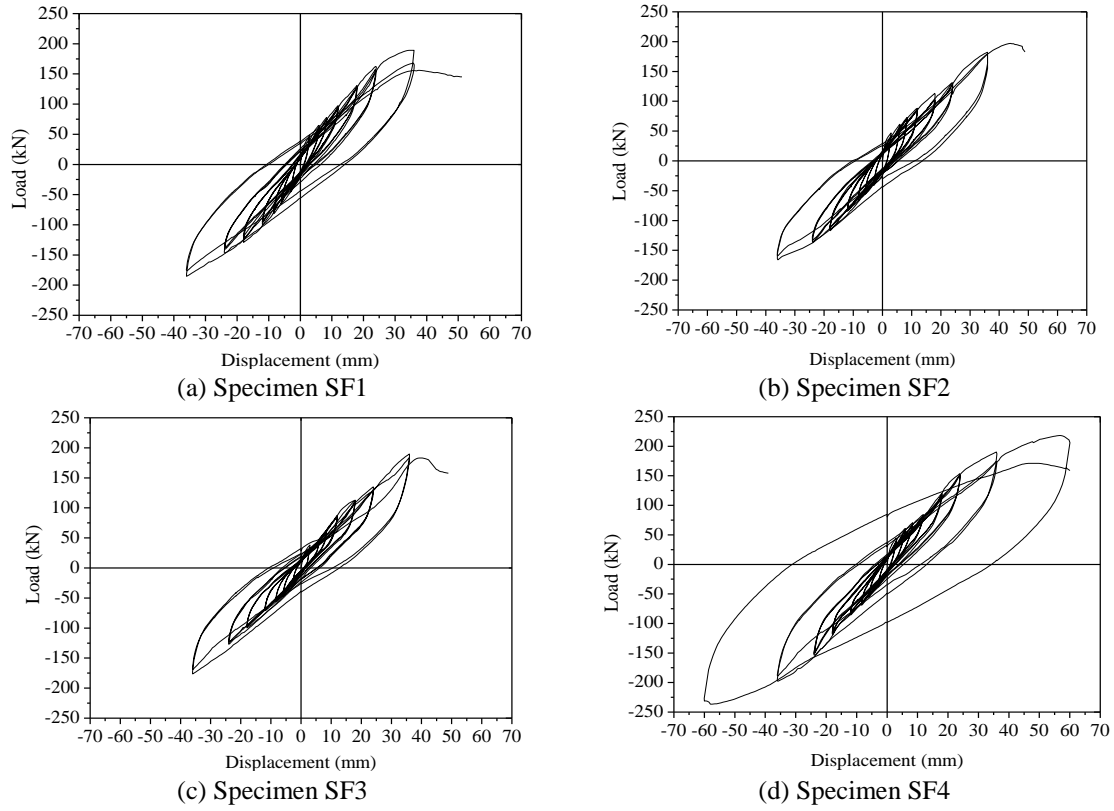
(a) Specimen SF1   (b) Specimen SF2

(c) Specimen SF3   (d) Specimen SF4
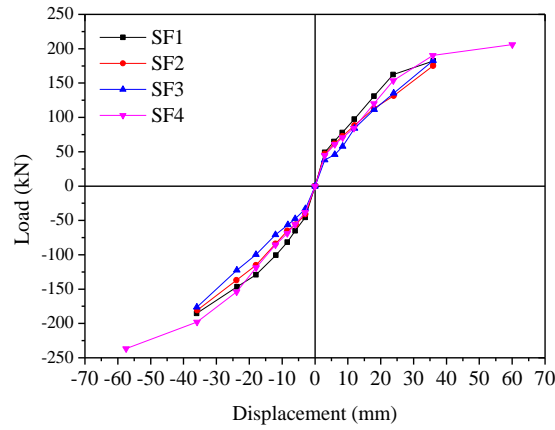
Fig. 8 Hysteretic responses of specimens

Fig. 9 Backbone curves of specimens with CL infill walls

3.2 Lateral stiffness

The lateral stiffness of each specimen gradually decreased with the increase of the beam end displacement. Stiffness reduction was caused by slippage between the steel connectors and the CL

infill wall and concrete damage near wall corners. In order to study the variation of specimen stiffness under cyclic loading, the lateral stiffness was evaluated as

$$K_j = \frac{\sum\limits_{i=1}^{n} P_j^i}{\sum\limits_{i=1}^{n} u_j^i} \qquad (5)$$

where P_j^i and u_j^i are the absolute maximum lateral load and the corresponding lateral displacement under the ith loading cycle, and n is the number of cycles. The initial lateral stiffness of the specimens with the CL infill walls ranged from 11 to 16 kN/mm, which was two to three times that of the bare frame specimen (Table 3). Specimen SF3 had the lowest lateral stiffness among all specimens because the ceramic concrete had lower elastic modulus (2.43×10^4 N/mm^2) than the normal-weight concrete (3.93×10^4 N/mm^2). The lateral stiffness of all specimens decreased significantly within a displacement level of $\Delta/\Delta_y=1$ (Fig. 10(a)), where the lateral stiffness reduced to about half of the initial value. In the subsequent loading cycles, K_j decreased slowly and reached a value about 4 kN/mm, which was 1/4~1/3 of the initial stiffness. Moreover, the lateral stiffness of the system was about 1.5 to 2 times that of the bare steel frame over the moderate deformation region, close to that of the bare steel frame over the high deformation region

Table 3 Lateral stiffness of specimens

Displacement Level	Cycle No.	Lateral Stiffness K (kN/mm)				
		SF1	SF2	SF3	SF4	SF5
0.25Δ_y	1	16.05	14.98	12.08	14.04	5.59
	2	15.06	13.66	11.01	12.71	5.56
0.5Δ_y	1	11.00	10.00	7.76	9.68	5.29
	2	10.33	9.34	7.51	9.29	5.30
0.7Δ_y	1	9.53	8.20	6.84	8.28	5.13
	2	9.10	8.07	6.92	7.98	5.11
1Δ_y	1	8.30	7.16	6.44	7.12	4.77
	2	8.06	7.09	6.47	6.85	4.74
	3	7.89	7.09	6.57	6.73	4.71
1.5Δ_y	1	7.25	6.37	5.87	6.66	-
	2	7.06	5.98	5.87	6.52	-
	3	6.86	6.15	5.81	6.43	-
2Δ_y	1	6.51	5.61	5.19	6.46	-
	2	6.24	5.52	5.25	6.27	-
	3	6.15	5.43	5.32	6.27	-
3Δ_y	1	5.28	4.85	5.09	5.41	-
	2	4.80	4.72	4.90	5.07	-
5Δ_y	1	-	-	-	3.85	-

(a) Stiffness Degradation   (b) Bending of a Bolt
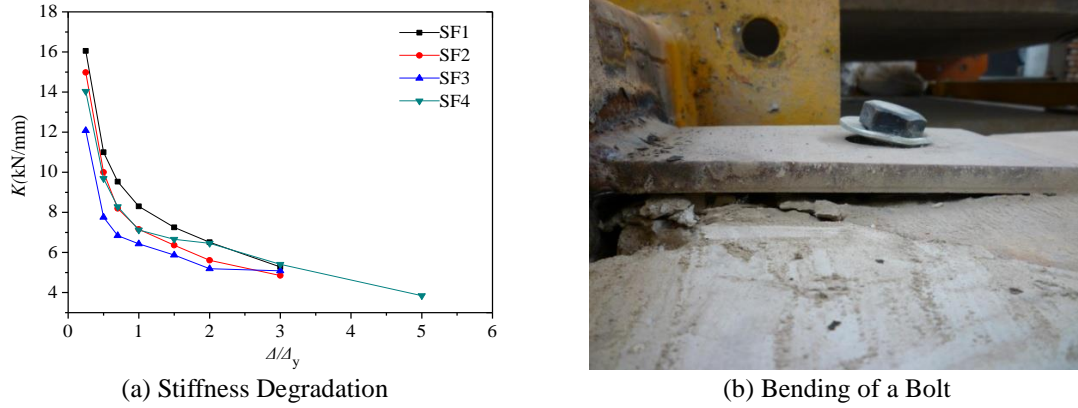
Fig.10 Stiffness degradation of specimens

($3\Delta_y$ to $5\Delta_y$). The lateral stiffness of Specimen SF4 did not vary much in the drift cycle from Δ_y (12 mm) to $2\Delta_y$ (24 mm), indicating that the diagonal steel straps could maintain the stiffness of the CL infill wall over the moderate deformation region and delay stiffness degradation of the wall up to a larger deformation region. Degradation of lateral stiffness became significant again when the bolt that connected the wall and the frame bent as shown in Fig. 10(b). Therefore, it is reasonable to ignore the contribution of the CL infill wall in the high deformation region, corresponding to the maximum considered earthquakes.

When the lateral displacement of the frame reached $0.25\Delta_y$, the boundary frame members remained elastic but the infill walls started to fracture. Therefore, the elastic lateral stiffness was calculated based on the test results up to $0.25\Delta_y$ cycles. The elastic lateral stiffness calculated based on Eq. (4) was 31.5 kN/mm for Specimens SF1 and SF2, and 23 kN/mm for Specimen SF3. The elastic lateral stiffness of Specimen SF5 (i.e., the bare frame) was 9.2 kN/mm according to the preliminary analysis of ABAQUS program. Based on the test results listed in Table 3, the comparison of stiffness varies from 65 to 124%. The difference is possibly due to the idealized boundary conditions assumed in analytical estimates. Note that the column base of actual specimens is not ideally fixed and the relative movement occurs between the infill walls and boundary fames due to slotted bolt holes in the infill-wall-to-boundary-frame connections. Such effects are not considered in Eq. (4), resulting in an overestimate in elastic stiffness.

3.3 Ductility factor

Ductility is a factor for evaluating the deformation capacity of structural members or systems. A displacement ductility factor, μ, which is defined as the ratio of the ultimate displacement, Δ_μ, to the yield displacement, Δ_{yo}, was adopted in this study to evaluate the seismic performance of the CL infill frame subjected to cyclic loading. The yield displacement, Δ_{yo}, and the ultimate displacement, Δ_μ, of the backbone curve are determined by using the method illustrated in Fig. 11, in which Δ_{yo} represents the displacement required to achieve a lateral load of P_m based on an initial slope of the backbone curve. The ultimate load is defined as $P_u=0.85P_m$, and the corresponding displacement is Δ_u. The characteristic points of each specimen are listed in Table 4.

Table 4 summarizes displacement ductility factors of the specimens. The displacement ductility factors of the specimens ranged from 4-4.5, indicating that the connections between the CL infill
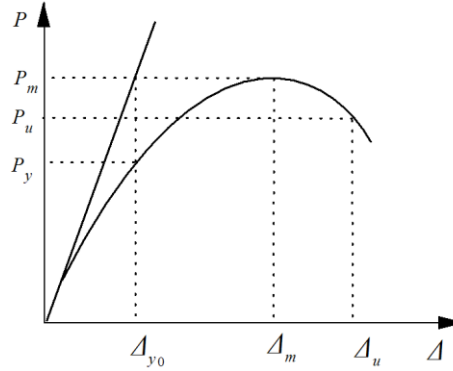
Fig. 11 Determination of feature points

walls and the boundary frame developed a stable level of ductility. Specimen SF4 had the maximum ductility capacity among all specimens because the steel straps not only provided confinement to the corner concrete but also helped resist the story shear. Table 4 also lists strength values of the specimens with infill walls. Based on the test results of Specimen SF5, the yield strength of the bare frame was about 62 kN. Note that the ultimate strength of the bare frame was unknown since the test of Specimen SF5 stopped at its yielding limit. It was observed that addition of the infill walls increases yield strength of the system on the order of 44.8 to 61.3%, depending upon the infill wall materials, distribution of the infill-wall-to-boundary frame connections and if diagonal straps were used in the infill wall. Although the systems tend to benefit from the added infill walls, it is recommended to conservatively neglect the infill walls in design unless future works develop a high-fidelity model to quantify the infill wall contributions and a reliable strategy for construction of the infill-wall-to-boundary-frame connections.

As listed in Table 4, the ultimate inter-story drifts are 3.2%, 3.3%, 3.2% and 4.2% for Specimens SF1, SF2, SF3 and SF4, respectively. The inter-story drift demands of a frame structure under DBE (Design Based Earthquake) and MCE (Maximum Considered Earthquake) motions depend on the seismicity of the construction site. According to the Chinese Code for Seismic Design of Buildings (GB50011-2010), the inter-story drift demands of a well-designed frame-wall system associated with DBE and MCE motions should be limited to 1 and 2%, respectively. Therefore, the infill walls and infill-wall-to-boundary-frame connections considered in this work can be used in the building frames to meet the inter-story drift requirements of the Chinese Code.

Table 4 Ductility factor for each specimen

Specimen ID.	Yield Limit		Maximum Strength		Ultimate Deformation		Ductility
	Δ_{yo} (mm)	P_y (kN)	Δ_m (mm)	P_m (kN)	Δ_u (mm)	P_u (kN)	μ
SF1	11.39	94.48	35.98	189.25	51.06 (3.2%)	160.86	4.5
SF2	12.36	89.70	35.93	196.94	54.09 (3.3%)	167.40	4.4
SF3	12.83	96.55	35.96	189.67	51.86 (3.2%)	161.22	4.0
SF4	14.47	99.87	56.72	218.11	65.65 (4.2%)	185.39	4.5

Note: Values in brackets are the inter-story drift

3.4 Hysteretic energy dissipation capacity

Hysteretic energy is an alternative index to response quantities like force or displacement ductility but includes the cumulative damage effect to structural members (Chou and Uang 2000, 2003). The equivalent viscous damping coefficient (ζ_{eq}) was adopted to analyze the energy capacity of the infilled steel frame under cyclic loads. The coefficient ζ_{eq} was calculated based on Eq. (6), in which S_{ABC} and S_{CDA} were the areas enclosed by curves ABC and CDA, respectively, in Fig. 12, and S_{OBE} and S_{ODF} were the areas within triangles OBE and ODF, respectively

$$\xi_{eq} = \frac{1}{2\pi} \frac{S_{ABC} + S_{CDA}}{S_{OBE} + S_{ODF}} \tag{6}$$

Except for Specimen SF4, all specimens failed at the beam end displacement of $5\Delta_y$ so the energy was not computed at that cycle. Fig. 13 shows that ζ_{eq} initially decreased with the increase of the beam end displacement, caused by the reduction of the lateral stiffness of the CL infill frame. In the yield stage ($1<\Delta/\Delta_y\leq2$), ζ_{eq} was around 0.1, near the lowest value in the tests. When $\Delta/\Delta_y\geq2$, ζ_{eq} increased with the increase of the beam end displacement due to plastic deformation of concrete in compression. The equivalent viscous damping coefficient ζ_{eq} reached 0.12-0.15 for all specimens at $\Delta/\Delta_y=3$. Note that due to the use of steel straps on both sides of the wall, the equivalent viscous damping coefficient ζ_{eq} was 0.22 at the beam end deformation of $\Delta/\Delta_y=5$.
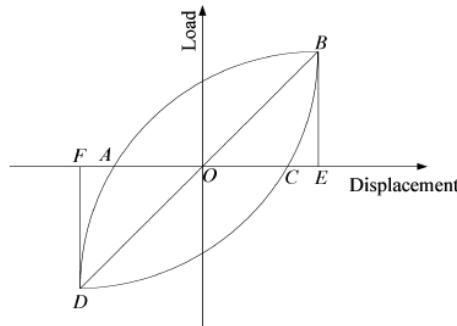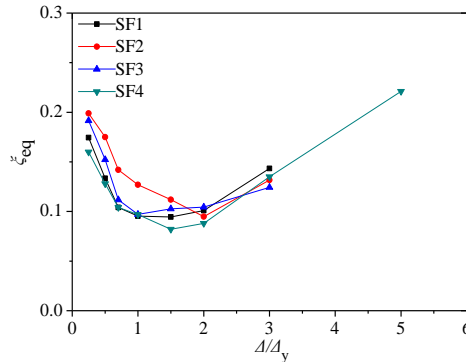

Fig. 12 Schematic of a hysteretic loop

Fig.13 Equivalent viscous damping coefficient

4. Conclusions

This paper presents the cyclic behavior of steel building frames with CL infill walls and semi-rigid beam-to-column connections. Five specimens with and without the CL infill walls were tested to evaluate the system behavior. Test parameters included locations of steel connectors, effect of diagonal steel straps added to the CL infill wall and concrete properties of the CL infill wall. The main conclusions are as follows:

• Typical damage of the CL infill frames in the tests included spalling and crushing of corner concrete near steel connectors. Although the corner concrete was damaged, the CL infill wall and the frame remained together till the end of the test due to the success of bolted connections, which allowed relative movement between the wall and the frame under lateral loads.

• The initial lateral stiffness of the steel frames with CL infill walls was two to three times that of the bare steel frame, but stiffness degradation was significant due to concrete damage and slippage between the connector and the infill wall. The lateral stiffness of the frames with CL infill walls was about 1.5 to 2 times that of the bare steel frame in the moderate deformation region and approached to that of the bare steel frame in the high deformation region ($3\Delta_y$ to $5\Delta_y$). The steel frame with the CL infill wall strengthened by the diagonal steel straps showed a lower level of stiffness degradation in the moderate deformation region, and its strength was increased by 8% compared with the same one but without diagonal steel straps. All specimens showed similar lateral stiffness in the large deformation region, irrespective of locations of steel connectors, concrete properties and if diagonal steel straps were used.

• Displacement ductility capacity of the specimens ranged from 4 to 4.5, and could be increased when the diagonal steel straps were added to the wall. Hysteretic energy dissipation capacity of the systems with CL infill walls, which was calculated by using the equivalent viscous damping coefficient, ζ_{eq}, decreased significantly in the low deformation region. Over the moderate deformation region, ζ_{eq} increased with the increase of the beam end deformation due to plastic deformation of concrete in compression and yielding or buckling of the steel beam. The equivalent viscous damping coefficient, ζ_{eq}, reached 0.12-0.15 at $\Delta/\Delta_y=3$ and 0.22 at $\Delta/\Delta_y=5$.

Acknowledgements

References

ATC 63 (2009), *Quantification of Building Seismic Performance Factors*, Applied Technology Council (ATC), Federal Emergency Management Agency.
ABAQUS (2009), *ABAQUS Analysis user's manual I-V*, Version 6.9, USA.
Aliaari, M. and Memari, A.M. (2005), "Analysis of masonry infilled steel frames with seismic isolator subframes", *Eng. Struct.*, **27**(4), 487-500.
Benayoune, A., Abdul Samad, A.A., Trikha, D.N., Abang Ali, A.A. and Ellinna, S.H.M. (2008), "Flexural behaviour of pre-cast concrete sandwich composite panel-experimental and theoretical investigations",

Constr. Build. Mater., **22**(4), 580-592.

Cavaleri, L. and Trapani, F.D. (2014), "Cyclic response of masonry infilled RC frames: experimental resultsand simplified modeling", *Soil Dyn. Earthq. Eng.*, **65**, 224-242.

Carrillo, J. and Alcocer, S. (2013), "Simplified equation for estimating periods of vibration of concrete wall housing", *Eng. Struct.*, **52**, 446-454.

Chou, C.C. and Uang, C.M. (2000), "Establishing absorbed energy spectra-an attenuation approach", *Earthq. Eng. Struct. Dyn.*, **29**(10), 1441-1455.

Chou, C.C. and Uang, C.M. (2003), "A procedure for evaluating seismic energy demand of framed structures", *Earthq. Eng. Struct. Dyn.*, **32**(2), 229-244.

El-Sokkary, H. and Galal, K. (2009), "Analytical investigation of the seismic performance of RC frames rehabilitated using different rehabilitation techniques", *Eng. Struct.*, **31**(9), 1955-1966.

Fang, M.J., Wang, J.F. and Li, G.Q. (2013), "Shaking table test of steel frame with ALC external wall panels", *J. Constr. Steel Res.*, **80**, 278-286.

GB50011-2010 (2010), *Chinese Code for Seismic Design of Buildings*, Ministry of Housing and Urban-Rural Development of the People's Republic of China. (in Chinese)

Hou, H.T., Hu, X.J., Li, G.Q. and Wang, Y.M. (2009), "Ultimate load-bearing capacity of the energy-saving composite sandwich panels", *J. Build. Mater.*, **12**(1), 106-111. (in Chinese)

Lee, H.S. and Ko, D.W. (2007), "Seismic response characteristics of high-rise RC wall buildings having different irregularities in lower stories", *Eng. Struct.*, **29**(11), 3149-3167.

Le, B.D. (2014), "Analytical study of partially-restrained steel frames with reinforced concrete infill walls subjected to cyclic loading", Department of Civil Engineering, National Taiwan University, Taipei, Taiwan.

Sun, G.H., He, R.Q., Gu, Q.A. and Fang, Y.Z. (2011), "Cyclic behavior of partially-restrained steel frame with RC infill walls", *J. Constr. Steel Res.*, **67**(12), 1821-1834.

Tong, X., Hajjar, J.F., Schultz, A.E. and Shield, C.K. (2005), "Cyclic behavior of steel frame structures with composite reinforced concrete infill walls and partially-restrained connections", *J. Constr. Steel Res.*, **61**(4), 531-552.

Wallace, J. and Wada, A. (2000), "Hybrid wall systems: US-Japan research", *Proceedings of 12th World Conference on Earthquake Engineering*, New Zealand.

CC